A Surface Plasmon Enhanced Infrared Photodetector Based on InAs Quantum Dots

Chun-Chieh Chang,[†] Yagya D. Sharma,[‡] Yong-Sung Kim,[†] Jim A. Bur,[†] Rajeev V. Shenoi,[‡] Sanjay Krishna,[‡] Danhong Huang,[§] and Shawn-Yu Lin*,[†]

[†]The Future Chips Constellation & Department of Physics, Applied Physics and Astronomy, Rensselaer Polytechnic Institute, Troy, New York 12180, [‡]Center for High Technology Materials, Department of Electrical and Computer Engineering, University of New Mexico, Albuquerque, New Mexico 87106, and [§]Space Vehicles Directorate, Air Force Research Laboratory, Kirtland Air Force Base, New Mexico 87117

ABSTRACT In this paper, we report a successful realization and integration of a gold two-dimensional hole array (2DHA) structure with semiconductor InAs quantum dot (QD). We show experimentally that a properly designed 2DHA-QD photodetector can facilitate a strong plasmonic−QD interaction, leading to a 130% absolute enhancement of infrared photoresponse at the plasmonic resonance. Our study indicates two key mechanisms for the performance improvement. One is an optimized 2DHA design that permits an efficient coupling of light from the far-field to a localized plasmonic mode. The other is the close spatial matching of the QD layers to the wave function extent of the plasmonic mode. Furthermore, the processing of our 2DHA is amenable to large scale fabrication and, more importantly, does not degrade the noise current characteristics of the photodetector. We believe that this demonstration would bring the performance of QD-based infrared detectors to a level suitable for emerging surveillance and medical diagnostic applications.

KEYWORDS Surface plasmon, quantum dots, infrared detection, subwavelength optics

Since the pioneering work of Ritchie in 1957, there has been a great deal of interest in confining light strongly at the metal surface by surface plasmons (SP).[1,2] The large number of photonic density-of-state at the metal−dielectric interface is particularly attractive for enhancing light−matter interaction and for improving the performance of light emission and detection.[3,4] However, to realize an active plasmonic device, the active element must be placed in the near-field regime and within the decay length of a plasmonic mode.[2] In 2004, Okamoto et al. successfully placed semiconductor quantum wells about 20 nm below a metal surface and observed an enhanced light emission.[3] Yet, an innovative approach is still needed to increase the wave function extent of a plasmonic mode and to facilitate active interaction. Furthermore, for light detection, the challenge remains as it demands an efficient coupling of light from the far-field into a localized surface plasmon.

In recent years, rapid progress has also been made in using plasmonic structures for achieving strong light focusing at the subwavelength regimes.[5−10] The advance in nanotechnology has also made it possible to make subwavelength, metallic two-dimensional hole arrays (2DHAs). This type of 2D hole array is unique as it can support the plasmonic modes and also facilitate light coupling through Bragg scattering.[5,6] Chang et al. utilized a metallic 2DHA to achieve a photoresponse line width narrowing.[11] However, they did not observe an enhancement of photoresponse due possibly to a relatively poor light coupling in their design and a low transmission due to the use of a thick metal film. Shenoi et al. also utilize a 2DHA photonic-crystal cavity and report a relative photoresponse enhancement by normalizing the long-wave to the midwave response.[12] No absolute enhancement of photoresponse was observed. Additionally, Yu et al. propose to use a 1D metallic grating for light coupling and a plasmonic slit 50nm wide to enhance infrared absorption. However, in their design, the use of a much wider grating of 200μm (4000 times larger than the slit width) increases the pixel size by a large amount to 200 μm.[13] The challenge of an efficient coupling of light into a plasmonic mode remains unresolved. Moreover, today, there is no successful experimental demonstration of an absolute enhancement of infrared photoresponse arising from the plasmonic−quantum dot interaction.

In this paper, we propose a new design and illustrate a successful realization of a monolithic integration of a gold 2DHA with active InAs QD layers. Using an optimized 2DHA for an efficient light coupling, we show experimentally that the 2DHA-QDIP can increase the photon−quantum dot interaction and lead to a more than 100% absolute enhancement of infrared photoresponse. Further enhancement is possible by optimizing the spatial overlaying between the QD layers and the plasmonic mode. We note that the processing of our metallic 2DHA structure is low cost, amenable to large scale fabrication, and, more importantly, does not degrade the noise current characteristics of the photodetector. We believe that this demonstration would bring the performance of QD-based infrared detectors to a
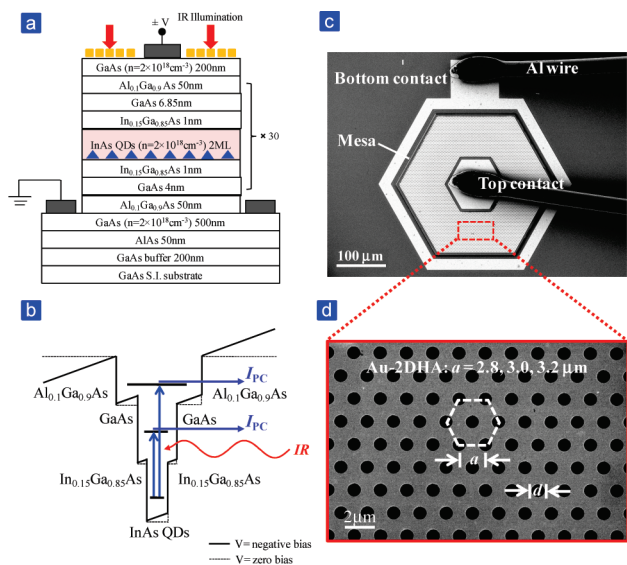
FIGURE 1. Design of 2DHA-QDIP for enhanced infrared detection. (a) A schematic of the 30-period QDIP sample structure. (b) A schematic energy band diagram of QDs in a well structure. The band structure is designed to respond to dual-band infrared excitation at $\lambda \sim 5$ and $9\ \mu$m, respectively. (c) A large area SEM image of the fabricated 2DHA-QDIP device. The device has a typical size of $300 \times 300\ \mu$m^2. (d) A zoom-in SEM image of the 2DHA. The lattice constant is $a = 2.8$, 3.0, and $3.2\ \mu$m, and the thickness of Au film is 50 nm.
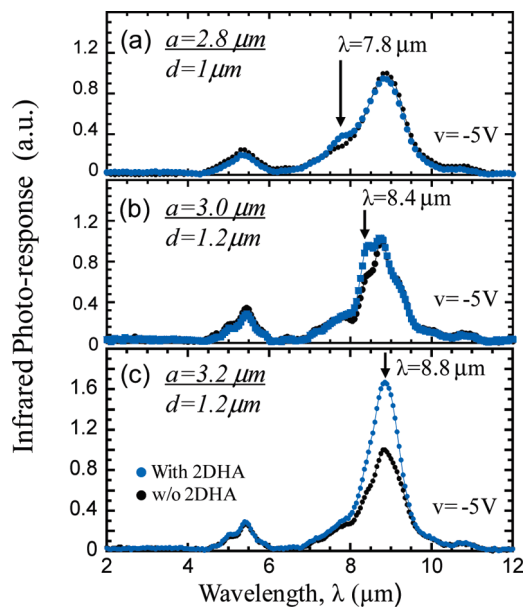

FIGURE 2. Spectral matching of plasmonic resonance to QD spectral response. Measured photoresponse spectra from three 2DHA-QD samples (the blue squares) with $a = 2.8$, 3.0, $3.2\ \mu$m, respectively. The spectra taken from QD samples with no 2DHA (the black dots) show two response maxima at $\lambda = 5.45$ and $8.8\ \mu$m, respectively. For the sample with $a = 2.8\ \mu$m, there is a weak kink at $\lambda = 7.8\ \mu$m (indicated by vertical arrow). As "a" is increased to 3.0 and $3.2\ \mu$m, the corresponding kink wavelength is shifted to $\lambda = 8.4$ and $8.8\ \mu$m, respectively. For the sample with $a = 3.2\ \mu$m, the photoresponse exhibits a maximum enhancement of 65% at $\lambda = 8.8\ \mu$m. The observed peak-λ scales linearly with "a" and is due to plasmonic resonance of the 2DHA.

level suitable for emerging surveillance and medical diagnostic applications.[12,14]

A schematic of our quantum dot infrared photodetector (QDIP) sample is shown in Figure 1a. A detailed description of it has been described earlier.[14,15] A similar QD sample with a plasmonic filter has also been realized recently for polarization-selective sensing purpose.[16] The sample is grown from a semi-insulating GaAs substrate and consists of a 30-period of QD layers imbedded inside $In_{0.15}Ga_{0.85}As$ quantum wells. The 30-period of QD layer has a total thickness of 2μm and is optimized for dual-band infrared absorption at $\lambda \sim 5$ and $\lambda \sim 9\ \mu$m, respectively.[14] A schematic of the energy band diagram of the QDs in a well structure is shown in Figure 1b. On top of the QDIP sample, we fabricate our metallic 2DHA structure using a combination of a standard optical lithography and a metal lift-off process. The 2DHA has the hexagonal lattice symmetry, a lattice constant $a = 2.5-3.72\ \mu$m, and a hole diameter of $d = 1.0-2.05\ \mu$m. In Figure 1c, we show a large area scanning electron microscopy (SEM) image of the fabricated 2DHA structure. The top and bottom electrical contacts as well as the mesa-isolation boundary are indicated in the figure. In Figure 1d, we show the zoom-in view of the 2DHA with a uniform 50 nm Au film. The lattice constant, or the nearest hole-to-hole spacing, is also indicated. The ability to vary the lattice constant allows us to tune the plasmonic resonant wavelength of the 2DHA[10] and to match it to the absorption peak of the QDs.

Once the device processing is completed, they are cleaved and wire-bonded to a chip carrier for electrical and optical characterization. The photoresponse measurement of our 2DHA-QDIP sample was carried out using a combination of a blackbody radiation source and a monochromator. The irradiance from the IR emitter was first modulated by an optical chopper, passing through the monochromator, and then incident on the detector mounted in a liquid N_2 cryostat. The photocurrent from the detector was amplified by a Keithley 428 current amplifier and fed to a SR 830 lock-in amplifier. The samples under test are typically reverse-biased at $V = 0$ to -5 V and the wavelength of the incident radiation was scanned over the infrared regime, $\lambda = 2-12\ \mu$m.

In parts a−c of Figure 2, we show photoresponse curves (the blue squares) taken from three 2DHA-QDIP devices with $a = 2.8$, 3.0, and $3.2\ \mu$m, respectively. For a more accurate comparison of device performance, we also fabricated a reference QDIP device (without the 2DHA) right next to each 2DHA-QDIP device and the data are shown as black dots. The photoresponse spectrum for $a = 2.8\ \mu$m sample (Figure 2a), exhibits two peaks at $\lambda = 5.45$ and $8.8\ \mu$m, corresponding to the two maxima of the QD absorption spectrum. The spectrum of the 2DHA-QDIP is nearly identical to the reference one with one exception, i.e., the appearance of a small, but clear kink at $\lambda = 7.8\ \mu$m. For the sample with a larger $a = 3.0\ \mu$m (Figure 2b), it also shows a spectrum similar to the reference. However, the amplitude of the kink becomes

stronger, and its wavelength shifts to a longer wavelength of $\lambda = 8.4\,\mu m$. As we continue to increase $a = 3.2\,\mu m$ (Figure 2c), the kink-λ approaches the QDIP absorption maximum at $\lambda = 8.8\,\mu m$ and we have achieved a nearly perfect spectral matching. In this case, the photoresponse exhibits a large, absolute enhancement of 65% at $\lambda = 8.8\,\mu m$ (or 165% signal amplitude as compared to the reference). It is noted that the resonant-λ shifts with "a", but is still within the main QD absorption band for samples with $a = 2.8-3.2\,\mu m$. Under this condition, the photoresponse is enhanced. Recognizing that the 2DHA only permits the transmission of a small fraction of light ($\sim$15%) into the QD layers, the observation of 165% photoresponse from the QDs is significant. These data show that the use of a metallic 2DHA with a thin metal of 50 nm can enhance the rate of photon−electron generation by a factor of 11 (i.e., 165%/ 15%).

It is noted that the kink wavelength in Figure 2 increases linearly with "a" of the metallic 2DHA. This suggests that the kink and the enhanced photoresponse may be correlated to the plasmonic resonance of the 2DHA.[10] To independently verify the resonance-λ, we fabricated a series of nominally the same 2DHA (with no QDs) and measured their transmittance spectra. We found that the resonant-λ of the 2DHA not only scales linearly with "a" but also agrees with the kink-λ observed in the photoresponse spectrum within 10%. This procedure confirms that the observed photoresponse enhancement is due to plasmonic resonance. Hence, by matching the plasmonic resonant wavelength of the 2DHA to the absorption peak of the QDs, the plasmonic−QD interaction is enhanced. Additionally, it is noted that when the lattice constant "a" is increased, the hole-filling fraction is decreased and the corresponding transmission amplitude (T) will also decrease. For our sample with $d = 1.2\,\mu m$, we found that $T = 31.9$, 20.2, and 14% for $a = 2.8$, 3.0, and 3.2μm, respectively.

It is known that the absorption process of our 2DHA-QD system may be described by Fermi's golden rule.[17,18] The photon−electron generation rate is given by the product of intraband matrix element of the QDs and the photon density-of-states[19−21] at the plasmonic resonance. Accordingly, the criteria for achieving an optimum photoresponse are (1) spectral matching of plasmonic resonance to QDIP absorption peak to increase density-of-state, (2) optimization of 2DHA design to improve transmittance to $\sim$100%, and (3) spatial matching of the plasmonic high field region to the active QD region to increase their mutual interaction. We now address the issue of optimizing the 2DHA transmittance. A detailed analysis of spatial mode matching will be discussed later.

In an attempt to increase transmission of incoming light and, meanwhile, to maintain the spectral matching condition, we fabricated a new set of 2DHA-QDIP samples. We also fabricated nominally the same 2DHA to check for light transmittance. In parts a−c of Figure 3, we show photore-
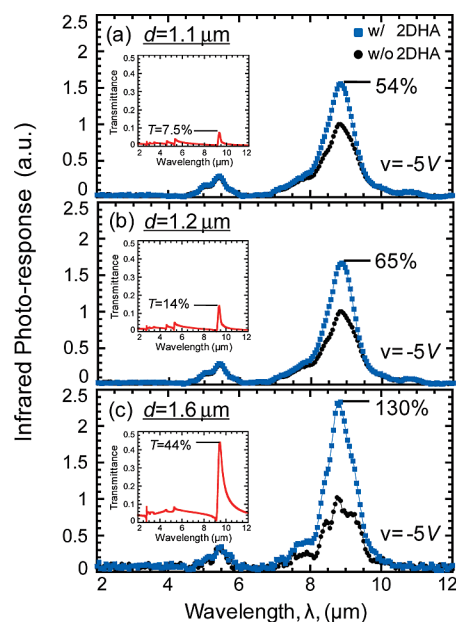

FIGURE 3. Design optimization of 2DHA to improve infrared transmission and photoresponse. The measured photoresponse spectra from 2DHA-QD samples (the blue squares) with the same $a = 3.2\,\mu m$, but three different $d = 1.1$, 1.2, 1.6 μm, respectively. The spectra taken from QD samples with no 2DHA (the black dots) are also presented. As "d" is increased from 1.1 to 1.2 to 1.6 μm, the photoresponse enhancement at $\lambda = 8.8\,\mu m$ is observed to be 54%, 65%, and 130%, respectively. In the inset, we show the corresponding transmission spectra of the 2DHA structures (the red curves). When d is increased from 1.1 to 1.6 μm, the transmittance increases significantly from 11% to 44%.

sponse curves taken from samples having the same $a = 3.2\,\mu m$, but different $d = 1.1$, 1.2, and 1.6 μm, respectively. All devices under test are biased at $V = -5$ V. The same "a" guarantees a good spectral matching and the different "d" is designed to control light transmittance through tunneling.[10] This is because the plasmonic resonance of our sample occurs at the metal−dielectric interface. So, at resonance, the incoming light would need to penetrate through the thin metallic 2D holes via evanescent tunneling. In the inset of Figure 3, we show the corresponding transmittance spectra (the red curves) of the 2DHA. First, the transmittance data show an encouraging trend, i.e., as "d" is increased from 1.1 to 1.2 to 1.6 μm, the sample's transmittance increases systematically from 11% to 15% to 44%. Second, the measured transmission peaks for all three samples are fixed at the same wavelength, as expected from the 2DHA plasmonic resonant condition.[10] Finally, the measured photoresponse for all three 2DHA-QDIP samples exhibits large enhancement at $\lambda \sim 8.8\,\mu m$ as compared to those without the 2DHA (the reference-QDIP). We note that the slight, but non-negligible difference in the response curves for the three reference-QDIPs, shown in Figure 3, may be due to growth nonuniformity and variation in sample fabrication from run to run. The photoresponse enhancement is observed to be 54%, 65%, and 130%, as "d" is increased from 1.1 to 1.2 to 1.6 μm, respectively. In our 2DHA-QDIP design, the
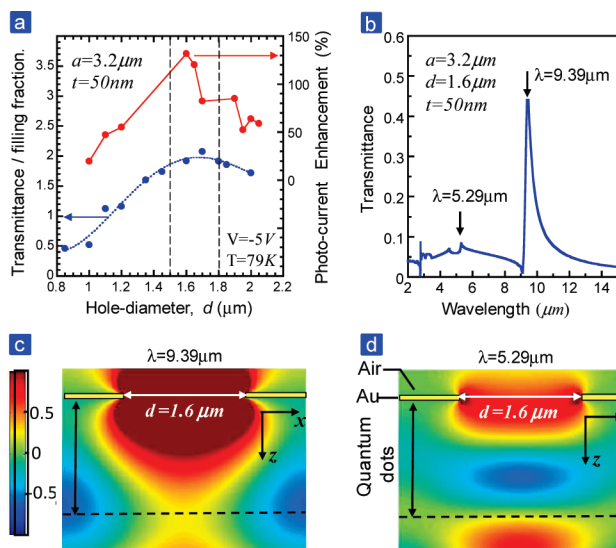
FIGURE 4. Origin of the photoresponse enhancement. (a) A plot of the photoresponse enhancement (red dots) and the EM transmission flux (blue dots) as a function of the hole diameter d ($a = 3.2$ μm). The photoresponse enhancement reaches its maximum value of 130% at $d = 1.6$ μm. The EM transmission flux exhibits a similar trend and reaches a peak value of 2.1 at $d = 1.6-1.7$ μm. (b) A computed transmittance spectrum for our optimized 2DHA structure, having $a = 3.2$ μm and $d = 1.6$ μm. The 2DHA supports a weak resonance at $\lambda = 5.29$ μm and a stronger resonance at $\lambda = 9.39$ μm. (c and d) A cross-sectional view of FDTD calculation result of the electric field in the vicinity of the 2D holes at $\lambda = 9.39$ μm and $\lambda = 5.29$ μm, respectively. The EM wave is incident along the z axis, and the electric field is linearly polarized along the x axis. The color scale denotes the normalized magnitude of the electric field.

capability to vary "a" and "d" independently allows us to simultaneously match the plasmonic and QDIP spectra and to optimize the 2DHA infrared transmission. The increase of an absolute enhancement of 130% in photoresponse (or a 230% signal strength) is believed to be the largest ever observed in the infrared-λ without having to etch the 2DHA into GaAs and the QD layer. We comment that the resonant peak-λ of a 2DHA is angular-dependent which can change its spectral aligment to the QD absorption band. Particularly, for a light incident angle of <30°, our samples show a moderate shift in its resonant-λ such that it is still well aligned to the main QD absorption band. For larger incident angles, the resonant-λ is shifted away from the main absorption band and would limit the detector's performance.

In Figure 4a, we summarize the photocurrent enhancement (red dots) and the EM transmittance flux (blue dots) and as a function of the hole diameter (d). The "transmittance flux" is defined as ratio of the measured transmission amplitude to the 2D-hole filling fraction (ff). The transmittance flux is greater than unity for $d > 1.1$ μm and reaches a peak value of 2 at $d = 1.6-1.7$ μm. This is the optimized hole-diameter range where the incident light is strongly focused and efficiently coupled into the device. The photocurrent data follow a similar trend. It is enhanced for all the tested samples with $d = 1.0-2.2$ μm and has a peak value of 130% at $d = 1.6$ μm. The close correlation of the two sets

of experimental data provides further evidence that the observed photocurrent enhancement is the result of a strong surface plasmonic field interacting with the QDs.

This observation prompts us to study the electric-field profile at the plasmonic resonances in the vicinity of the 2D holes. In Figure 4b, we show a computed transmittance spectrum for our optimized 2DHA structure, having $a = 3.2$ μm and $d = 1.6$ μm. The 2DHA supports a weak resonance at $\lambda = 5.29$ μm and a stronger resonance at $\lambda = 9.39$ μm. This calculated resonance wavelength is about 8% larger than the $\lambda = 8.8$ μm observed in the photoresponse measurement and may be due to the nature of QD—plasmonic interaction.[22] In Figure 4c, we show the electric-field profile (E_x) obtained at $\lambda = 9.39$ μm by a finite-difference time-domain method. The strong field region (the dark red color with field-enhancement of >200% as compared to the incident field) not only extends laterally along the entire hole area ($d = 1.6$ μm) but also penetrates deep into the substrate of ~0.8 μm. We recall that our 2DHA-QD sample has 30 periods of QD layer and a thickness of 2 μm. Therefore, about 40% of the QDs are within the high field region, leading to a strong interaction between the EM field and the QDs. For comparison purpose, in Figure 4d, we show the electric-field profile near the 2D holes at another resonance wavelength $\lambda = 5.29$ μm. In this case, the field around the 2D holes is much weaker. The relatively weaker field is consistent with the transmittance data shown in Figure 4b. It also provides a clear explanation of the photocurrent data shown in Figures 2 and 3. Namely, a high plasmonic field at $\lambda \sim 9$ μm gives a strong enhancement in photocurrent generation, whereas a relatively weak plasmonic field at $\lambda \sim 5$ μm yields a negligible enhancement.

Here, we briefly comment on the impact of 2DHA processing on the noise—current density of our infrared photodetector. The noise—current density measurement was performed using a fast Fourier transform (FFT) analyzer with a 300 K scene for a voltage bias of $V = -5$ to 5 V.[14,15] The term "noise—current density" is defined as $(i_n/(\Delta f)^{1/2})$ and has a unit of "A/Hz$^{1/2}$". It is also inversely proportional to a detector's detectivity: $D^* \propto R_p/(i_n/(\Delta f)^{1/2})$, a measure of a detector's signal-to-noise ratio. Here, i_n, Δf, and R_p are the noise current, frequency bandwidth, and photoresponsivity of a photodetector, respectively. In parts a and b of Figure 5, we show the measured noise current density for samples with (the blue curve) and without (the black curve) 2DHA for both $d = 1.6$ and 1.2 μm, respectively. The data demonstrate that the noise current density is essentially the same for samples with and without 2DHA over the entire bias range. Hence, we can conclude that while the photoresponse signal of the 2DHA-QDIP is increased at the resonance, its noise current density is not affected significantly by the 2DHA fabrication.

Next, we model the optimum performance enhancement of our 2DHA-QD plasmonic detector by spatially matching the QD layer to the plasmonic high field region. In Figure 6,
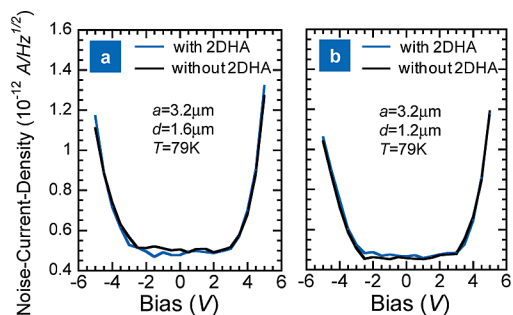
FIGURE 5. Noise current density measurements of the 2DHA-QDIP samples. (a and b) The noise current density data measured at $T = 79$ K for samples with (the blue curve) and without the 2DHA (the black curve) for 2DHA hole diameters $d = 1.6$ and 1.2 μm, respectively.
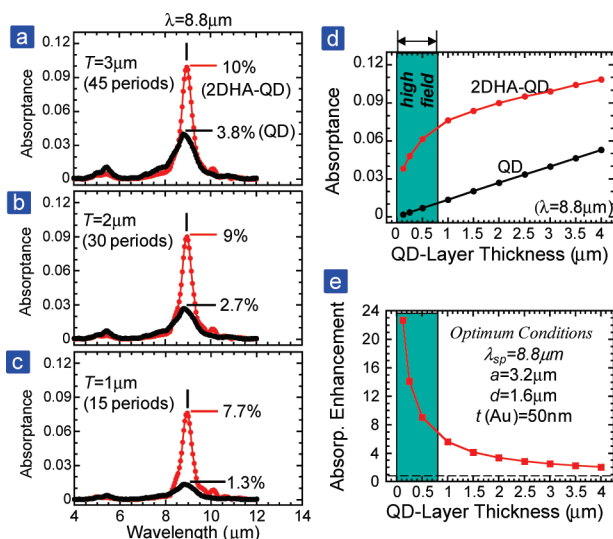

FIGURE 6. Optimum conditions for plasmonic−QD interaction. (a−c) The calculated absorption spectra of a 2DHA-QD sample (the red curves) with three different QD layer thicknesses, $T = 3$, 2, and 1 μm, respectively. The spectra for the QD samples, shown as the black curves, are for reference. The enhanced QD absorption occurs at $\lambda \sim 9$ μm, i.e., the plasmonic-λ of the 2DHA structure. (d) A summary plot of peak absorptance as a function of T for the 2DHA-QD (the red circles) and the QD (the black circles) samples. The green color indicates the region where a strong plasmonic-field exists. (e) A plot of absorption enhancement as a function of T for an optimum 2DHA-QD sample ($a = 3.2$ μm, $d = 1.6$ μm, and $t = 50$ nm). The data show that an enhancement of as much as 10 times can be achieved at $T = 0.5$ μm.

we show the absorption spectra of the QDs with (the red curves) and without (the black curves) the Au 2DHA structure. The calculation was done using the transfer matrix method[23] and assuming a complex dielectric function, $\varepsilon(\lambda) = \varepsilon_1(\lambda) + i\varepsilon_2(\lambda)$, for the QD layer. The dielectric function is justified as it reproduces a peak absorption value of 2.7 % that agrees with a previously measured data.[24] Also, the Au 2DHA has a film thickness of $t = 50$ nm, a plasmonic resonance at $\lambda \sim 9$ μm, and a vertical spatial extent of $\Delta z \sim 0.8$ μm.

In Figure 6a, we show the result of an absorptance spectrum calculated for a sample with a total QD-layer thickness of $T = 3$ μm or 45 QD layers. The spectrum exhibits a peak absorption of 10 % at $\lambda \sim 9$ μm for the 2DHA-QD sample, which is 2.5 times higher than that for the QD sample (3.8 %). The selective enhancement of QD absorption at the plasmonic wavelength confirms the occurrence of the plasmon−QD interaction. For the $T = 2$ μm samples (Figure 6b), the respective peak absorption for the QD and 2DHA-QD samples is 2.7 % to 9 %, giving a larger enhancement of 3.3 times. Systematically, we continue to reduce the QD-layer thickness T. For the $T = 1$ μm samples (Figure 6c), the respective peak absorption for the QD and 2DHA-QD samples is now 1.3−7.7 % and shows a larger enhancement of 6 times. From these data, we conclude that as the QD-layer thickness is reduced, a better spatial matching is achieved and a larger absorption enhancement observed.

In Figure 6d, we summarize this observation by plotting the peak absorption vs QD-layer thickness for both the QD (the black circles) and 2DHA-QD (the red circles) samples. For the QD samples, the intraband absorption is low (<5 %) and the value of the peak absorptance scales linearly with QD thickness. For the 2DHA-QD sample, the peak absorption rises quickly as a function of T for $T < 0.8$ μm, increases more linearly for $T > 2$ μm, and reaches a value of 11 % at $T = 4$ μm. The fast rise in QD-absorption occurs precisely at the region where a strong plasmonic-field exists (as indicated by the green color region). These data are significant as it reveals the importance of spatial matching between the QD layer and the plasmonic mode. In Figure 6e, we plot the absorption enhancement (i.e., absorption (2DHA-QD)/absorption (QD)) as a function of T. The plot shows that a 20 fold absorption enhancement is theoretically possible. We note that a QDIP sample can have a thin QD active regime of 0.132 μm and, at the same time, a high detectivity of 8×10^{10} Jones.[25] Our data also show that enhancements of even 5 and 10 times can be achieved by using moderate thicknesss of $T = 1.3$ and 0.5 μm, respectively.

In summary, we have realized an integrated 2DHA-QD sample for infrared detection. We have also successfully demonstrated a more than 100 % enhancement of infrared photoresponse and detectivity at the plasmonic resonance. Furthermore, we identify three criteria for achieving an optimum plasmonic−QD interaction: (1) spectral matching of plasmonic resonance to QD spectral response; (2) tunneling optimization to improve light transmittance through subwavelength holes; and (3) spatial matching of the vertical extend of plasmonic field to the QD region. By doing so, it is possible to achieve a factor of 10 enhancement in infrared photoresponse and detectivity. This would bring the performance of QD infrared detector to a level that is compatible to the widely used, conventional MCT infrared detector.

NANO LETTERS

Supporting Information Available. Plasmonic dispersion of gold 2DHA samples. This material is available free of charge via the Internet at http://pubs.acs.org.

REFERENCES AND NOTES

(1) Ritchie, R. H. *Phys. Rev.* **1957**, *106*, 874–881.

(2) Raether, H. *Surface Plasmons*; Springer: Berlin, 1988.

(3) Okamoto, K.; Niki, I.; Shvartser, A.; Narukawa, Y.; Mukai, T.; Scherer, A. *Nat. Mater.* **2004**, *3*, 601–605.

(4) Tsai, M.-F.; Chuang, T.-H.; Meng, C.-Y.; Chang, Y.-C.; Lee, S.-C. *Appl. Phys. Lett.* **2006**, *89*, 173116.

(5) Barnes, W. L.; Dereux, A.; Ebbesen, T. W. *Nature* **2003**, *424*, 824–830.

(6) Ozbay, E. *Science* **2006**, *311*, 189–193.

(7) Pendry, J. B.; Martin-Moreno, L.; Garcia-Vidal, F. J. *Science* **2004**, *305*, 847–848.

(8) Garcia-Vidal, F. J.; Martin-Moreno, L. *Phys. Rev. B* **2002**, *66*, 155412.

(9) Laux, E.; Genet, C.; Skauli, T.; Ebbesen, T. W. *Nat. Photonics* **2008**, *2*, 161–164.

(10) Chang, J. C.-C.; Yang, Z.-P.; Huang, D.-H.; Cardimona, D. A.; Lin, S.-Y. *Opt. Lett.* **2009**, *34*, 106–108.

(11) Chang, C. Y.; Chang, H. Y.; Chen, C. Y.; Tsai, M. W.; Chang, Y. T.; Lee, S. C.; Tan, S. F. *Appl. Phys. Lett.* **2007**, *91*, 163107.

(12) Shenoi, R. V.; Ramirez, D. A.; Sharma, Y.; Attaluri, R. S.; Rosenberg, J.; Painter, O.; Krishna, S. http://copilot.caltech.edu/research/SPDet/PlasmonPhC-ver2.pdf.

(13) Yu, Z.; Veronis, G.; Fan, S. *Appl. Phys. Lett.* **2006**, *89*, 151116.

(14) Krishna, S. *J. Phys. D: Appl. Phys.* **2005**, *38*, 2142–2150.

(15) Berger, P. R.; Chang, K.; Bhattacharya, P.; Singh, J.; Bajaj, K. K. *Appl. Phys. Lett.* **1988**, *53*, 684–686.

(16) Rosenberg, J.; Shenoi, R. V.; Vandervelde, T. E.; Krishna, S.; Painter, O. *Appl. Phys. Lett.* **2009**, *95*, 161101.

(17) Merzbacher, E. *Quantum Mechanics*; John Wiley & Sons: New York, 1997.

(18) Choi, K. K. *The Physics of Quantum Well Infrared Photodetectors*; World Scientific: Singapore, 1997.

(19) Purcell, E. M. *Phys. Rev.* **1946**, *69*, 681.

(20) Yablonovitch, E. *Phys. Rev. Lett.* **1987**, *58*, 2059–2062.

(21) John, S. *Phys. Rev. Lett.* **1987**, *58*, 2486–2489.

(22) Schaadt, D. M.; Feng, B.; Yu, E. T. *Appl. Phys. Lett.* **2005**, *86*, No. 063106.

(23) Li, Z.-Y.; Lin, L.-L. *Phys. Rev. E* **2003**, *67*, No. 046607.

(24) Gunapala, S. D.; et al. *IEEE. J. Quantum Electron.* **2007**, *43*, 230–237.

(25) Attaluri, R. S.; et al. *J. Vac. Sci. Technol., B* **2006**, *24*, 1553–1555.